ANALYSIS OF MAGNETOHYDRODYNAMIC (MHD) NANOFLUID FLOW WITH HEAT AND MASS TRANSFER OVER A POROUS STRETCHING SHEET

A.S. ODESOLA, I.O. ABIALA*, F.O. AKINPELU and O.J. FENUGA
Department of Mathematics, Faculty of Science, University of Lagos
Akoka, Lagos, NIGERIA
E-mails: sotontop@yahoo.com; iabiala@unilag.edu.ng; foakinpelu@yahoo.co.uk;
ofenuga@unilag.edu.ng

This work investigates a three-dimensional Magnetohydrodynamic (MHD) nanofluid flow with heat and mass transfer over a porous stretching sheet. Firstly, partial differential equations are transformed into coupled non-linear ordinary differential equations through a similarity variables transformation and solved by Galerkin Finite Element Methods (FEM). The effects of thermal radiation, viscous dissipation and chemical reaction on the fluid flow are considered. The behaviour and properties of pertinent flow parameters on the velocity, temperature and concentration profiles are presented and discussed graphically. The effects of the friction coefficient parameter, Nusselt and Sherhood numbers are also shown and considered using tables. The work is in good agreement in comparison with the recent work in literature.

Key words: finite element method, heat and mass transfer, MHD, nanofluid flow, porous stretching sheet.

1. Introduction

The study of MHD boundary layer flow on a continuous stretching sheet has attracted considerable attention in recent years due to its enormous applications in industrial manufacturing processes such as the aerodynamics, extrusion of plastic sheets, liquid film, hot rolling, wire drawing, glass fibre, paper production, drawing of plastic films, metal and metal spinning (Freidoonimehr and Rahimi [1]).

The main limitation of conventional heat transfer fluids, i.e. H_2O, ethylene glycol, oil, etc., is their low thermal conductivity. Since the thermal conductivity of these fluids plays an important role and effects the heat transfer coefficient between the medium and the surface, innovative techniques for improving heat transfer by using ultra-fine solid particles in the fluids have been used extensively for the last several years (Kumar *et al.*[2]).

Choi [3] introduced the addition of solid nanoparticles and base fluids to form nanofluids. Nanofluids have been found to possess additional thermo-physical properties, such as thermal diffusivity, thermal conductivity, viscosity, (Asker *et al.* [4]; Nadeem *et al.*[5]; Yu *et al*. [6]; Xuan and Li [7]).

Choi *et al*. [8] proved in their experimental investigation that the thermal conductivity of the base fluid is enhanced approximately twice by dispersing nanoparticles with volume fraction of nanoparticles less than 1 per cent.

Oahimire *et al*. [9] investigated the effects of thermal diffusion and thermal radiation on unsteady heat and mass transfer by free convective MHD micropolar fluid flow bounded by a semi – infinite vertical plate in a slip – flow regime under the action of a ransverse magnetic field. The results showed that the observed parameters have a significant influence on the flow, heat and mass transfer.

---

* To whom correspondence should be addressed

Ganesh *et al*. [10]studied the influence of a magnetic field on natural convective flow of a nanofluid past a semi-infinite stretching sheet. They observed non-metallic nanoparticles (TiO_2 and Al_2O_3) and metallic nanoparticles (Cu and Ag) and found that velocity of metallic nanoparticles was lower than that of non-metallic nanoparticles when water was taken as a base fluid.

Jalilpour *et al*. [11]carried out an investigation for MHD stagnation point flow of a nanofluid past a heated porous stretching sheet with suction/injection conditions and prescribed surface heat flux. The impact of thermophoresis and Brownian motion can be seen in the transport equations. The leading coupled PDEs are non-dimensionalized and deciphered analytically by HPM (Homotopy Perturbation Method) using the Padé method. Chamkha *et al*. [12] presented the heat and mass transfer characteristics of nanofluid under different geometries like single and doubled-driven square cavities, porous cavity heated by a thick triangular wall, wedge and vertical cone, respectively. Sudarsana Reddy *et al*. [13] made a heat transfer analysis of Ag–water and Cu–water nanofluids over a rotating disk.

Fenuga *et al*. [14] presented an analysis of a thermal boundary layer flow over a vertical plate with electrical conductivity and convective surface boundary conditions. The Runge – Kutta fourth order method with shooting technique was used in solving the equations. Makinde *et al*. [15] numerically studied MHD reacting and radiating 3-D flow of a Maxwell fluid past a stretching sheet with heat source/sink and Soret effects in a porous medium.

2. Model formulation

Consider a steady, three-dimensional, viscous incompressible, laminar MHD layer flow of a nanofluid over a stretching sheet through a medium filled with water-based alumina nanofluid situated at $z=0$. It is also assumed that (u,v and w) are the velocity components along the (x, y and z) directions respectively.
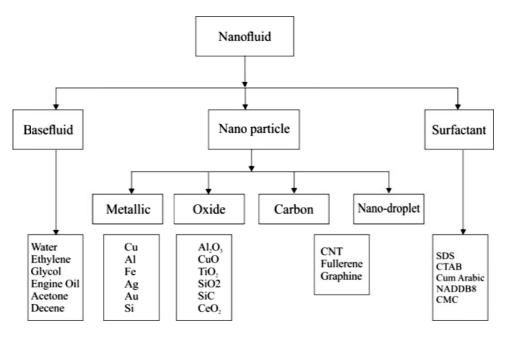

Fig.1. Schematic diagram of types of nanofluid.

The following assumptions were made:
(i)   a constant magnetic field of strength B_0 in the $z-$ direction is considered;
(ii) the magnetic Reynolds number is deficient so that the induced magnetic field is neglected;
(iii) the applied electrical field is ignored;

(iv) the thermal radiation, Soret and first ordered destructive chemical reaction are considered.

The flow is caused by the stretching of the sheet that moves in its own plane with the surface velocity *ax* and *by*, where *a* and *b* are stretching constants.

Under the above assumptions, using the Boussinesq and boundary layer approximations, the governing equations describing the continuity, momentum, energy and concentration in the presence of thermal radiation, viscous dissipation and chemical reaction take the following form
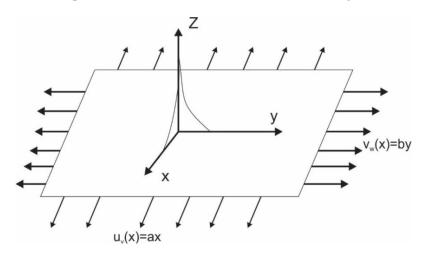

Fig.2. Physical model and coordinate system.

Continuity equation

$$\frac{\partial u}{\partial x} + \frac{\partial v}{\partial y} + \frac{\partial w}{\partial z} = 0 \ . \tag{2.1}$$

Momentum equation

$$u\frac{\partial u}{\partial x} + v\frac{\partial u}{\partial y} + w\frac{\partial u}{\partial z} = \frac{\mu_{nf}}{\rho_{nf}}\frac{\partial^2 u}{\partial z^2} - \frac{\sigma B_0^2}{\rho_{nf}}u - \frac{\mu_{nf}}{\rho_{nf}}\frac{1}{K}u + g\beta_T\left(T - T_\infty\right) + g\beta_C\left(C - C_\infty\right), \tag{2.2}$$

$$u\frac{\partial v}{\partial x} + v\frac{\partial v}{\partial y} + w\frac{\partial v}{\partial z} = \frac{\mu_{nf}}{\rho_{nf}}\frac{\partial^2 v}{\partial z^2} - \frac{\sigma B_0^2}{\rho_{nf}}v - \frac{\mu_{nf}}{\rho_{nf}}\frac{1}{K}v \ . \tag{2.3}$$

Energy equation

$$u\frac{\partial T}{\partial x} + v\frac{\partial T}{\partial y} + w\frac{\partial T}{\partial z} = \alpha_{nf}\frac{\partial^2 T}{\partial z^2} - \frac{1}{\rho C_\rho}\frac{\partial q_r}{\partial z} + \frac{\mu_{nf}}{\left(\rho C_\rho\right)_{nf}}\left(\frac{\partial u}{\partial z}\right)^2 +$$

$$+ \frac{\sigma B_0^2}{\rho_{nf}}u^2 + \tau\left\{D_B\left(\frac{\partial T}{\partial z}\frac{\partial C}{\partial z}\right) + \frac{D_T}{T_\infty}\left(\frac{\partial T}{\partial z}\right)^2\right\} + Q\left(T - T_\infty\right). \tag{2.4}$$

Chemical reaction equation

$$u\frac{\partial C}{\partial x} + v\frac{\partial C}{\partial y} + w\frac{\partial C}{\partial z} = D\frac{\partial^2 C}{\partial z^2} - \frac{D_T}{T_\infty}\frac{\partial^2 T}{\partial z^2} - K\left(C - C_\infty\right). \tag{2.5}$$

The associated boundary conditions are as follows

$$u = ax + \gamma \frac{\partial u}{\partial z}, \quad v = bx + \gamma \frac{\partial v}{\partial z}, \quad w = -u_0, \quad T = T_w, \quad c = c_w \quad \text{at} \quad z = 0,$$

$$u \to 0, \quad v \to 0, \quad T \to T_\infty, \quad c \to c_\infty \quad \text{as} \quad z = \infty.$$

(2.6)

In order to solve Eqs (2.1)-(2.6), the following similarity variables were employed (Reddy *et al.* 2017)

$$u = axf'(\eta), \quad v = byg'(\eta), \quad w = -(av)^{1/2}(f+g)(\eta), \quad \eta = z\sqrt{\frac{a}{v}}, \quad \theta(\eta) = \frac{T - T_\infty}{T_w - T_\infty},$$

(2.7)

$$h(\eta) = \frac{C - C_\infty}{C_w - C_\infty}$$

where $\theta(\eta)$ is the dimensionless temperature and $h(\eta)$ is the dimensionless concentration.

Upon substituting the similarity variables into Eqs (2.2)-(2.5), the following system of ordinary differential equations was obtained.

$$f'''(\eta) + (f(\eta) + Sg(\eta))f''(\eta) - (f'(\eta))^2 - f'(\eta)(M + K_1) + G_r\theta(\eta) + G_r h(\eta) = 0,$$ (2.8)

$$g'''(\eta) + (f(\eta) + Sg(\eta))g''(\eta) - (g'(\eta))^2 - g'(\eta)(M + K_1) = 0,$$ (2.9)

$$\theta''(\eta)\left(\frac{3 + 4R}{3P_r R}\right) + P_r(f(\eta) + g(\eta))\theta'(\eta) + N_t(\theta'(\eta))^2 +$$

$$+ N_b\theta'(\eta)h'(\eta) + \delta P_r\theta(\eta) + P_r E_c(f''(\eta))^2 + MP_r(f'(\eta))^2 = 0,$$

(2.10)

$$h''(\eta) + Le(f(\eta) + g(\eta))h'(\eta) + \frac{N_t}{N_b}\theta''(\eta) - LeG_r h(\eta) = 0.$$ (2.11)

The corresponding boundary conditions are

$$f(0) = 0, \quad f'(0) = 1 + \gamma f''(0), \quad g(0) = 0, \quad g'(0) = S + \gamma g''(0),$$

$$\theta'(0) = -B_{it}(1 - \theta(0)), \quad h'(0) = -B_{ic}(1 - h(0)) \quad \text{at} \quad \eta = 0$$

(2.12)

$$f'(\infty) \to 0, \quad g'(\infty) \to 0, \quad \theta(\infty) \to 0, \quad h(\infty) \to 0.$$ (2.13)

3.1. Variational formulation of the problem

In order to obtain a compatible variational form of the problem, the orders of Eqs (2.8)-(2.13) are then reduced using the approach of Reddy (2006), such that the non-linear variables f' and g' are re-written as

$$f' = r \,,\tag{3.1}$$

$$g' = t \,.\tag{3.2}$$

Hence, the system of Eqs (2.8) – (2.13) becomes

$$r''(\eta) + \left(f(\eta) + Sg(\eta)\right) r'(\eta) - \left(r(\eta)\right)^2 - r(\eta)(M + K_1) + G_r\theta(\eta) + G_r h(\eta) = 0 \,,\tag{3.3}$$

$$t''(\eta) + \left(f(\eta) + Sg(\eta)\right) t'(\eta) - \left(t(\eta)\right)^2 - t(\eta)(M + K_1) = 0 \,,\tag{3.4}$$

$$\theta''(\eta)\left(\frac{3 + 4R}{3 P_r R}\right) + P_r\left(f(\eta) + g(\eta)\right)\theta'(\eta) + N_t(\theta'(\eta))^2 + N_b\theta'(\eta)h'(\eta) +$$
$$+ \delta P_r\theta(\eta) + P_r E_c\left(r'(\eta)\right)^2 + M P_r\left(r(\eta)\right)^2 = 0,\tag{3.5}$$

$$h''(\eta) + Le\left(f(\eta) + g(\eta)\right) h'(\eta) + \frac{N_t}{N_b}\theta''(\eta) - LeG_r h(\eta) = 0 \,,\tag{3.6}$$

and the associated boundary conditions become

$$f(0) = 0, \quad r(0) = 1 + \gamma r'(0), \quad g(0) = 0, \quad t(0) = S + \gamma t'(0),\tag{3.7}$$

$$\theta'(0) = -B_{it}\left(1 - \theta(0)\right), \quad h'(0) = -B_{ic}\left(1 - h(0)\right) \quad \text{at} \quad \eta = 0$$

$$r(\infty) \to 0, \quad t(\infty) \to 0, \quad \theta(\infty) \to 0, \quad h(\infty) \to 0 \,.\tag{3.8}$$

The variational form associated with Eqs (3.1) – (3.6) over a typical element, over a two noded linear element (X_e, X_{e+1}), employing the approach used by Swapna *et al.* (2016), is given by the following;

$$\int_{X_e}^{X_{e+1}} N_1\left[f'(\eta) - r\right] dX = 0,\tag{3.9}$$

$$\int_{X_e}^{X_{e+1}} N_2\left[g'(\eta) - t\right] dX = 0,\tag{3.10}$$

$$\int_{X_e}^{X_{e+1}} N_3\left[r''(\eta) + \left(f(\eta) + Sg(\eta)\right) r'(\eta) - \left(r(\eta)\right)^2 - r(\eta)(M + K_1) +\right.$$
$$\left. + G_r\theta(\eta) + G_r h(\eta)\right] dX = 0,\tag{3.11}$$

$$\int_{X_e}^{X_{e+1}} N_4\left[t''(\eta)+\left(f(\eta)+Sg(\eta)\right)t'(\eta)-(t(\eta))^2-t(\eta)(M+K_1)\right]dX=0, \tag{3.12}$$

$$\int_{X_e}^{X_{e+1}} N_5\left[\theta''(\eta)\left(\frac{3+4R}{3P_r R}\right)+P_r\left(f(\eta)+g(\eta)\right)\theta'(\eta)+N_t(\theta'(\eta))^2\right.+$$
$$\left.+N_b\theta'(\eta)h'(\eta)+\delta P_r\theta(\eta)+P_r E_c(r'(\eta))^2+MP_r(r(\eta))^2\right]dX=0, \tag{3.13}$$

$$\int_{X_e}^{X_{e+1}} N_6\left[h''(\eta)+Le\left(f(\eta)+g(\eta)\right)h'(\eta)+\frac{N_t}{N_b}\theta''(\eta)-LeG_r h(\eta)\right]dX=0 \tag{3.14}$$

where N_1,N_2,N_3,N_4,N_5 and N_6 are the weight functions and may be viewed as the variations in f,r,g,t,θ and h, respectively.

3.2. Derivation of the finite element equations

The finite element model may be obtained from Eqs (3.9)-(3.14) by using finite element approximation of the form

$$f=\sum_{j=1}^{2}f_j\psi_j, \quad r=\sum_{j=1}^{2}r_j\psi_j, \quad g=\sum_{j=1}^{2}g_j\psi_j, \quad =\sum_{j=1}^{2}t_j\psi_j, \quad \theta=\sum_{j=1}^{2}\theta_j\psi_j, \quad h=\sum_{j=1}^{2}h_j\psi_j \tag{3.15}$$

where $N_1=N_2=N_3=N_4=N_5=N_6=\psi_j=(j=1,2)$ are the interpolation functions for the linear elements (X_e,X_{e+1}) and $f_j^{\,e},g_j^{\,e},\theta_j^{\,e}$ and $h_j^{\,e}$ are the velocity, temperature and concentration, respectively, at the jth node of a typical e^{th} element (X_e,X_{e+1}) and $\psi_j^{\,e}$ the shape function for this element (X_e,X_{e+1}) is taken as

$$\psi_1^{\,e}=\frac{X_{e+1}-X}{X_{e+1}-X_e} \quad \text{and} \quad \psi_2^{\,e}=\frac{X-X_e}{X_{e+1}-X_e}, \quad X_e\le X\le X_{e+1}. \tag{3.16}$$

The finite model of the equations for the eth element thus formed is given by

$$\begin{bmatrix}[k^{11}] & [k^{12}] & [k^{13}] & [k^{14}] & [k^{15}] & [k^{16}]\\ [k^{21}] & [k^{22}] & [k^{23}] & [k^{24}] & [k^{25}] & [k^{26}]\\ [k^{31}] & [k^{32}] & [k^{33}] & [k^{34}] & [k^{35}] & [k^{36}]\\ [k^{41}] & [k^{42}] & [k^{43}] & [k^{44}] & [k^{45}] & [k^{46}]\\ [k^{51}] & [k^{52}] & [k^{53}] & [k^{54}] & [k^{55}] & [k^{56}]\\ [k^{61}] & [k^{62}] & [k^{63}] & [k^{64}] & [k^{65}] & [k^{66}]\end{bmatrix}\begin{Bmatrix}f^e\\ r^e\\ g^e\\ t^e\\ \theta^e\\ h^e\end{Bmatrix}=\begin{Bmatrix}p^{1e}\\ p^{2e}\\ p^{3e}\\ p^{4e}\\ p^{5e}\\ p^{6e}\end{Bmatrix} \tag{3.17}$$

where $\left[K^{mn}\right],\{f^e\},\{r^e\},\{g^e\},\{t^e\},\{\theta^e\},\{h^e\}$ and $\{p^{me}\}, \{m,n = 1,2,3,4,5,6\}$ are the set of matrices and are defined as follows

$$K^{11} = \int_{X_e}^{X_{e+1}} \psi_i \frac{d\psi_j}{d\eta} d\eta, \quad K^{12} = -\int_{X_e}^{X_{e+1}} \psi_i \psi_j d\eta, \quad K^{13} = K^{14} = K^{15} = K^{16} = 0,$$

$$K^{22} = \int_{X_e}^{X_{e+1}} \psi_i \frac{d\psi_j}{d\eta} d\eta, \quad K^{23} = -\int_{X_e}^{X_{e+1}} \psi_i \psi_j d\eta, \quad K^{21} = K^{24} = K^{25} = K^{26} = 0,$$

$$K^{31} = -\int_{X_e}^{X_{e+1}} \psi_i \psi_j \frac{d\psi_j}{d\eta} d\eta, \quad K^{32} = \int_{X_e}^{X_{e+1}} -S\psi_i \psi_j \frac{d\psi_j}{d\eta} d\eta + (M+K_I)\psi_j\psi_j + \overline{r}\psi_j\psi_j,$$

$$K^{33} = -S\int_{X_e}^{X_{e+1}} \psi_i \frac{d\psi_j}{d\eta} d\eta, \quad K^{34} = 0, \quad K^{35} = -G_r\int_{X_e}^{X_{e+1}} \psi_i\psi_j d\eta,$$

$$K^{36} = -G_s\int_{X_e}^{X_{e+1}} \psi_i\psi_j d\eta, \quad K^{42} = -N_b\int_{X_e}^{X_{e+1}} \psi_i \frac{d\psi_j}{d\eta} d\eta,$$

$$K^{44} = (M+K_I)\int_{X_e}^{X_{e+1}} \left[(M+K_I)\psi_i\psi_j + \overline{t}\psi_i\psi_j - S\psi_i\psi_j\right] d\eta,$$

$$K^{51} = K^{53} = -P_r\int_{X_e}^{X_{e+1}} \psi_i \frac{d\psi_j}{d\eta} d\eta, \quad K^{52} = -P_r\int_{X_e}^{X_{e+1}} \left[M\overline{r}\psi_i\psi_j + \psi_i \frac{d\psi_j}{d\eta}\right] d\eta, \quad K^{54} = 0,$$

$$K^{55} = -\int_{X_e}^{X_{e+1}} \left[\delta P_r\psi_i\psi_j + N_b\psi_i \frac{d\psi_j}{d\eta} + N_t\overline{\theta}\psi_i \frac{d\psi_j}{d\eta} + P_r\psi_i\psi_j \frac{d\psi_j}{d\eta}\right] d\eta,$$

$$K^{61} = K^{63} = -L_e\int_{X_e}^{X_{e+1}} \psi_i \frac{d\psi_j}{d\eta} d\eta, \quad K^{62} = K^{64} = 0, \quad K^{65} = -\frac{N_t}{N_b}\int_{X_e}^{X_{e+1}} \frac{d\psi_i}{d\eta}\frac{d\psi_j}{d\eta} d\eta,$$

$$K^{66} = -L_e\int_{X_e}^{X_{e+1}} \left[C_r\psi_i\psi_j - \psi_i\psi_j \frac{d\psi_j}{d\eta}\right] d\eta, \quad P^{1e} = P^{2e} = 0, \quad P^{3e} = \left[\eta\psi_i \frac{dr}{d\eta}\right]_{X_e}^{X_{e+1}},$$

$$P^{4e} = \left[\eta\psi_i \frac{dt}{d\eta}\right]_{X_e}^{X_{e+1}}, \quad P^{5e} = \left[\frac{3+4R}{3P_rR}\right]\left[\eta\psi_i \frac{d\theta}{d\eta}\right]_{X_e}^{X_{e+1}}, \quad P^{6e} = \left[\eta\psi_i \frac{dh}{d\eta}\right]_{X_e}^{X_{e+1}}.$$

4. Results and discussion

The assembled equations obtained are solved using any of the numerical techniques, namely, the Gauss elimination method, LU decomposition method, etc. The shape functions used to approximate actual functions is of importance. The entire flow domain is divided into 10.000 quadratic elements of equal size and every aspect is two-noded, so the whole field contains 20.001 nodes. We have to evaluate four functions f, g, θ and h at every node. We obtained 80.004 non-linear equations after the assembly of element equations. After applying the given boundary conditions, the remaining system of non-linear equations is solved by using the Gauss elimination method with an accuracy of 0.00001 maintained. Gaussian quadrature is implemented for solving the integrations. The computer program of the algorithm was executed in MATHEMATICA 10.0 running on a PC. To investigate the sensitivity of the solutions to mesh density, we have performed the grid invariance test for velocity, temperature and concentration distributions, as shown in Tab.1. It is observed from this table that in the same domain, the accuracy is not affected, and even the number of elements increased by decreasing the size of the elements.

Comprehensive numerical computations are conducted for different values of the parameters that describe the flow characteristics and the results are illustrated graphically.

A representative set of computational results is presented in Figs 3-6. The thermo–physical properties of water and nanoparticles are shown in Tab.1. A comparison of the present results with the results reported by Hayat *et al*. [16] has been made and found consistent, as is shown in Tab.2.

Table 1. Thermo-physical properties of water and nanoparticles Das and Jana [17].

Fluid	$\rho\left(\dfrac{Kg}{m^3}\right)$	$C_p\left(\dfrac{J}{K_gK}\right)$	$k\left(\dfrac{W}{mK}\right)$	$\beta\,x\,10^5\left(K^{-1}\right)$
Pure water	*997.1*	*4,179*	*0.613*	*21*
Copper (Cu)	*8,933*	*385*	*401*	*167*
Silver (Ag)	*10,500*	*235*	*429*	*189*
Alumina (Al$_2$O$_3$)	*3970*	*765*	*40*	*0.85*
Titanium Oxide (TiO$_2$)	*4,250*	*686.2*	*8.9538*	*0.9*

Table 2. Comparison of (-θ (*0*)) with previously published data.

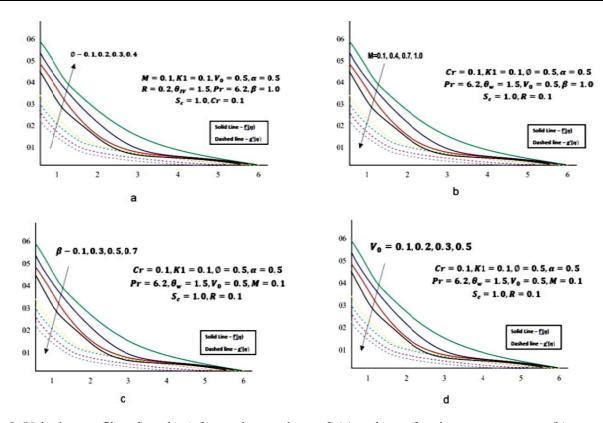| M	Parameter θ_w	R	$-\theta''(0)$	
			Hayat *et al*. (2015)	Present study
0.1	*1.1*	*0.1*	*0.74084*	*0.74081*
0.3	*1.1*	*0.1*	*0.70977*	*0.70975*
0.5	*1.1*	*0.1*	*0.68279*	*0.69281*
0.1	*1.2*	*0.1*	*0.74410*	*0.74413*
0.1	*1.3*	*0.1*	*0.74775*	*0.74776*
0.1	*1.4*	*0.1*	*0.75180*	*0.75182*
0.1	*1.1*	*0.05*	*0.73328*	*0.73329*
0.1	*1.1*	*0.15*	*0.74802*	*0.74801*
0.1	*1.1*	*0.2*	*0.75482*	*0.75483*

Fig.3. Velocity profiles *f'* and *g'* for various values of (a) volume fraction parameter φ, (b) magnetic parameter *M*, (c) velocity slip parameter and (d) suction parameter.
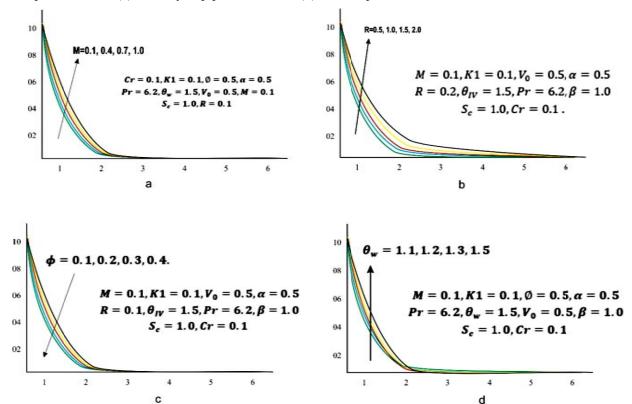

Fig.4. Temperature profiles *u* for various values of (a) volume fraction parameter φ, (b) magnetic parameter *M*, (c) temperature parameter and (d) radiation parameter.
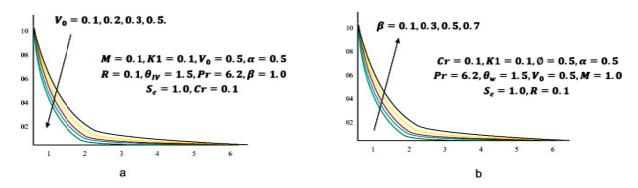
Fig.5.Temperature profiles θ for various values of (a) suction parameter V0 and (b) velocity slip parameter *b*.

   The concentration distributions for various values of the nanoparticle volume fraction φ, suction parameter (V0), velocity slip parameter (b) and chemical reaction parameter (Cr) are depicted in Figs 6a-d, respectively. It is noticed from Figs 6a and b that the concentration profiles decrease with the increasing values of nanoparticle volume fraction φ and suction parameter (V0) in the nanofluid. An increase in the values of the velocity slip parameter (b) increases the solutal boundary layer thickness in the boundary layer regime [Fig.6c]. Figure 6d shows that the concentration profiles are highly influenced and decrease with the chemical reaction parameter in the flow regime.
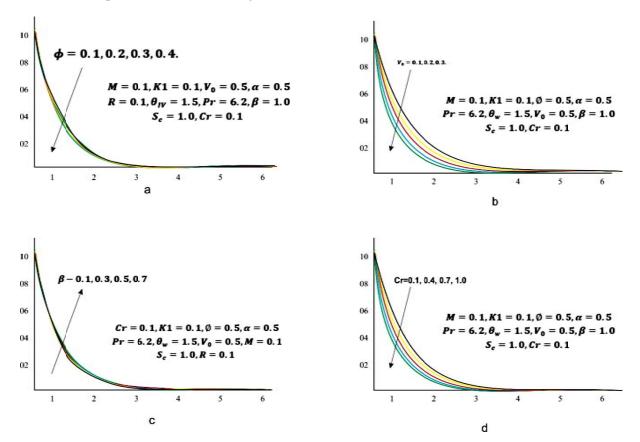

Fig.6. Concentration profiles *S* for various values of (a) volume fraction parameter *f,* (b) suction parameter V0, (c) velocity slip parameter *b* and (d) chemical parameter cr.

Table 3. The values of the skin friction coefficient ($f''(0)$ along the x direction, skin friction coefficient ($g''(0)$ along the y– direction, Nusselt number ($-u$, $h(0)$ and Sherwood number ($-S'(0)$) for different values of θ, V_0 and β.

φ	V_0	β	$f''''(0)$	$g''(0)$	$-θ''(0)$	$-S''(0)$
0.1	0.5	1.0	-0.465405	-0.221279	0.953875	0.538901
0.4	0.5	1.0	-0.437013	-0.207472	1.018023	0.562917
0.7	0.5	1.0	-0.399428	-0.189562	1.092812	0.594689
1.0	0.5	1.0	-0.361674	-0.172096	1.165039	0.625896
0.1	0.5	1.0	-0.465491	-0.221341	0.750102	0.543008
0.1	0.2	1.0	-0.485181	-0.232735	0.836987	0.615064
0.1	0.3	1.0	-0.504933	-0.244038	0.926619	0.692405
0.1	0.5	1.0	-0.543917	-0.265949	1.112660	0.861667
0.1	0.5	0.1	-0.949914	-0.429223	1.218382	0.665998
0.1	0.5	0.3	-0.763691	-0.351956	1.102273	0.608956
0.1	0.5	0.5	-0.642979	-0.300220	1.024832	0.571745
0.1	0.5	0.7	-0.557446	-0.262743	0.968601	0.545254

5. Conclusion

This work addressed the three - dimensional Magnetohydrodynamic (MHD) nanofluid flow with heat and mass transfer over a porous stretching sheet. The set of basic governing equations has been solved numerically using the finite element method. The numerical solutions have been developed for velocity, temperature, concentration, skin – friction, rate of heat and mass transfer coefficients. The features of the flow characteristics were analyzed by plotting graphs and discussed in detail.

- The influence of the Grashof number on heat and mass transfer stabilizes the momentum boundary layer growth.
- The concentration reduces with an increase in the Schmidt number.
- The velocity as well as concentration decrease with an increase in the chemical reaction parameter.
- The numerical results are obtained and compared with previously reported cases available in the literature and they are found to be in very good agreement.

Nomenclature

a − stretching rate(constant)
C_{fx} − skin-friction coefficient in the x-direction
C_{fx} − skin-friction coefficient in the y-direction
C_p − specific heat at constant pressure
f − nanoparticle volume fraction
K − porous parameter
K^* − mean absorption coefficient
k_0 − rate of chemical reaction
k_s − thermal conductivity of nanoparticle
M − magnetic parameter
Nu_x − Nusselt number

Pr   − Prandtl number
R − radiation parameter
Re_x − local Reynolds number in the x –direction
Re_y − local Reynolds number in the y-direction
Sc   − Schmidt number
Sh_x − Sherwood number
q_r − radiative heat flux
T − temperature of the fluid
T_w − uniform constant temperature
T_1 − free stream temperature
U_0 − suction parameter
u − velocity in the x-direction
u_w − temperature parameter
v − velocity in the y-direction
w − velocity in the z-direction
(x, y, z) − Cartesian coordinates

References

[1] Freidoonimehr, Navid Rahimi, Asghar (2018): *Brownian motion effect on heat transfer of a three-dimensional nanofluid flow over a stretched sheet with velocity slip*. − Journal of Thermal Analysis and Calorimetry. 135. 10.1007/s10973-018-7060-y.

[2] Kumar K.G., Gireesha B.J., Rudraswamy N.G. and Krishnamurthy M.R. (2019): *An unsteady flow and melting heat transfer of aNanofluid over a stretching sheet embedded in a porous medium*. − Int. J. of Applied Mechanics and Engineering, vol.24, No.2,pp.245-258

[3] Choi S.U.S. (1995): *Enhancing thermal conductivity of fluids with nanoparticle*. − In: D.A. Siginer, H.P. Wang(Eds.), Developments and Applications of Non-Newtonian Flows, The ASME New York, FED, vol.231/MD, vol.66, pp.99-105.

[4] Asker, Hamada, Elbashbeshy E. and Abdelgaber, Khaled (2018): *Heat and mass transfer of a Maxwell nanofluid over a stretching surface with variable thickness embedded in porous medium*. − International Journal of Mathematics and Computational Science, vol.4, No.3, pp.86-98.

[5] Nadeem S. and Akram S. (2011): *Magnetohydrodynamic peristaltic flow of a hyperbolic tangent fluid in a vertical asymmetric channel with heat transfer*. − Acta Mech. Sin.,vol.27, No.2, pp.237-250.

[6] Yu, Wei, HuaqingXie and Wei Chen (2010): *Experimental investigation on thermal conductivity of nanofluids containing graphene oxide nanosheets*. − Journal of Applied Physics, vol.107, No.9: 094317.

[7] Xuan Y. and Roetzel W. (2000): *Conceptions for heat transfer of nanofluids*. − International Journal of Heat and Mass Transfer, vol.43, pp.3701-3707.

[8] Choi S., Zhang Z.G., Yu W., Lockwood F.E. and Grulke E.A. (2009): *anomalous thermal conductivity enhancement on nanotube suspensions*. − Appl. Phys. Lett., vol.79, pp.2252-2254.

[9] Oahimire J.I., Olajuwon B.I., Waheed M.A. and Abiala I.O. (2013): *Analytical solution to MHD micropolar fluid flow past a vertical plate in a slip-flow regime in the presence of thermal diffusion and thermal radiation*. − Journal of the Nigerian Mathematical Society, vol.32, pp.33-60.

[10] Ganesh N.V., Ganga B. and Hakeem A.A. (2014): *Lie symmetry group analysis of magnetic field effects on free convective flow of a nanofluid over a semi-infinite stretching sheet*. − Journal of the Egyptian Mathematical Society, vol.22, No.2, pp.304-310.

[11] Jalilpour B., Jafarmadar S., Ganji D.D., Shotorban A.B. and Taghavifar H. (2014): *Heat generation/absorption on MHD stagnation flow of nanofluid towards a porous stretching sheet with prescribed surface heat flux*. − Journal of Molecular Liquids, vol.195, pp.194-204.

[12] Chamkha A.J. and Rashad A.M. (2015): *Unsteady heat and mass transfer by MHD mixed convection flow from a rotating vertical cone with chemical reaction and Soret and Dufour effects*. − Can. J. Chem. Eng., vol.92, pp.758-767.

[13] Sudarsana Reddy P., Sreedevi P. and Chamkha A.J. (2017): *MHD boundary layer flow, heat and mass transfer analysis over a rotating disk through porous medium saturated by Cu-water and Ag-water nanofluid with chemical reaction*. − Powder Technol., vol.307, pp.46-55.

[14] Fenuga O.J., Abiala I.O. and Salawu S.O. (2018): *Analysis of thermal boundary layer flow over a vertical plate with electrical conductivity and convective surface boundary conditions*. − Physical Science International Journal, vol.17, No.2, pp.1-9.

[15] Makinde O.D. and Animasaun L. (2016): *Thermophoresis and Brownian motion effects on MHD bioconvection of nanofluid with nonlinear thermal radiation and quartic chemical reaction past an upper horizontal surface of a paraboloid of revolution*. − Journal of Molecular Liquids, vol.221, pp.73-743.

[16] Hayat T., Hussain M., Alsaedi A., Shehzad S.A. and Chen G.Q. (2015): *Flow of power-law nanofluid over a stretching surface with Newtonian heating*. − J. Appl. Fluid Mech., vol.8, pp.273-280.

[17] Das S. and Jana R.N. (2015): *Natural convective magneto-nanofluid flow and radiative heat transfer past a moving vertical plate*. − Alexandria Engineering Journal, vol.54, pp.55-64.